Carbon 148 (2019) 317–325

Contents lists available at ScienceDirect

Carbon

journal homepage: www.elsevier.com/locate/carbon

Composite graphene-metal microstructures for enhanced multiband absorption covering the entire terahertz range

Longfang Ye [a, b, *, 1], Fang Zeng [a, 1], Yong Zhang [c], Qing Huo Liu [d]

[a] Institute of Electromagnetics and Acoustics, And Department of Electronic Science, Xiamen University, Xiamen, 361005, China
[b] Shenzhen Research Institute of Xiamen University, Shenzhen, 518057, China
[c] School of Electronic Science and Engineering, University of Electronic Science and Technology of China, Chengdu, Sichuan, 611731, China
[d] Department of Electrical and Computer Engineering, Duke University, Durham, 27708, USA

ARTICLE INFO

Article history:
Received 14 January 2019
Received in revised form
18 March 2019
Accepted 27 March 2019
Available online 30 March 2019

ABSTRACT

We numerically demonstrate a novel route to effectively enhancing multi-band terahertz absorption enabled by a variety of tunable polarization-insensitive multiband terahertz absorbers based on composite graphene and metal microstructures. In these devices, the multiband plasmon resonance absorption in graphene, resulted from the Fabry–Pérot cavity between the continuous graphene and the underneath metal reflector, can be effectively enhanced by the designed metal microstructures. As a demonstration, we simulate several multiband absorbers based on composite graphene and several patterned metal microstructures (spiral, ring, disk, square). It is interesting to find that the number of absorption bands can be arbitrarily manipulated by the dielectric spacer hight. By setting the same spacer height of 60 μm, all absorbers exhibit identical absorption properties with six near-unity absorption bands in the whole terahertz region ranging from 0.1 to 10.0 THz under normal incidence regardless of the shapes of microstructures. These absorption bands also show clear independence of polarization under normal incidence and the absorbance peaks can be flexibly adjusted by changing the graphene chemical potential. Our work opens up a new avenue for the development of various multi-band graphene absorbers, which may have enormous potential applications in terahertz photoelectric detectors, sensors, modulators, and switches.

1. Introduction

Terahertz wave generally refers to the electromagnetic wave with a frequency range of 0.1–10 THz, which has broad application prospects in many fields such as broadband communication, spectrum analysis, detection, imaging, and sensing [1–3]. In 2008, Landy et al. first demonstrated the concept of perfect microwave absorber [4]. To meet the demand of various practical applications, the frequency of absorber has been extended to terahertz, infrared, and visible of the spectrum [5–7]. A typical metamaterial absorber is made up of a three-layer structure with subwavelength metal subwavelength-structure array, a dielectric spacer, and a metal reflector. The near-unity absorption properties are usually achieved by the device ohmic loss and dielectric loss while remaining no transmission and reflection of the incident waves. Recently, multi-band terahertz absorbers have attracted increasing attention. For example, Kearney et al. proposed a multiband absorber composed of a periodic array of Aluminum (Al) squares with different sizes, SiO_x spacer, and Al ground for terahertz sensor applications [8]. Appasani et al. demonstrated a multi-band terahertz absorber with a split square ring resonator [9]. Wang et al. proposed a quad-band terahertz absorber formed by an asymmetric resonator [10], and a six-band terahertz absorber using a dual-layer stacked resonance structure [11]. However, due to the use of conventional metal and dielectric materials, such multi-band absorbers suffer from the non-tunable characteristics after fabrication. Therefore, how to achieve tunable multi-band terahertz perfect absorbers has become an important research direction in terahertz science and technology.

Graphene is a two-dimensional crystal made up of a single layer of carbon atoms bonded together in a hexagonal lattice, which has promising mechanical, electrical, and optical properties including

* Corresponding author. Institute of Electromagnetics and Acoustics, And Department of Electronic Science, Xiamen University, Xiamen, 361005, China.
E-mail address: lfye@xmu.edu.cn (L. Ye).
[1] These authors contributed equally to this work.

https://doi.org/10.1016/j.carbon.2019.03.086
0008-6223/

fast carrier mobility, high optical transparency, and tunability [12]. Taking the advantages of supporting surface plasmon polaritons (SPPs) in the terahertz and infrared ranges [13–15], graphene has been widely applied in the tunable terahertz and infrared plasmonic devices such as absorbers, waveguides, modulators, switches, metalens, and photodetectors [16–26]. In order to enhance the absorption of the incident electromagnetic waves, various absorbers with periodically patterned graphene disks, ribbons, squares [27–30], multilayer graphene [31], perforated graphene cavities [32] have been investigated. As we know, tunable multi-band terahertz absorbers are highly desirable in some specific terahertz trapping, imaging, and sensing applications. In recent years, some dual-, triple-, and multi-band graphene-based absorbers have been proposed and studied. For example, Zhang et al., Yao et al., and Zhou et al. proposed several dual- and triple-band absorbers composed of different shaped graphene patterns [33–35]. Gao et al. investigated a multiband terahertz absorber made up of multiple graphene ring arrays [36]. Wang et al. demonstrated an ultra-multiband absorber covering terahertz to mid-infrared regime based on metal gratings-dielectric-graphene sandwich structure [37]. However, most of the previously reported absorbers suffer from some drawbacks such as a small number of absorption bands, low absorption strength, and narrow frequency tuning range. Especially, development of tunable multi-band terahertz absorbers with perfect absorption and arbitrarily controllable number of absorption bands remain a challenge.

In this paper, we proposed multi-band terahertz graphene tunable polarization-insensitive absorbers with near-unity absorption based on hybrid graphene and metal microstructures. In these absorber designs, multi-band absorption is obtained from the Fabry–Pérot cavity between the continuous graphene and the underneath metal reflector. We incorporate metal microstructure arrays into that graphene-dielectric-metal reflector structure based absorber to achieve drastically enhanced multi-band terahertz absorption via the strong plasmon resonance effects induced by the designed metal microstructures. It is found that the number of absorption bands can be arbitrarily controlled by appropriately setting the height of the dielectric spacer between the graphene and the metal reflector. As a demonstration, we numerically simulate several multiband absorbers based on composite graphene with differently patterned metal microstructures (spiral, ring, disk, square). The simulated results clearly show that all absorbers demonstrate exactly the same absorption properties with six near-unity absorbance bands in the entire terahertz frequency region ranging from 0.1 to 10.0 THz no matter which kind of microstructures is used. In addition, such high absorption characteristics show clear independence of polarization under normal incidence and their absorbance peaks can be flexibly adjusted by changing the graphene Fermi level. The proposed concept provides a new method to enhance the multi-band terahertz absorption, which may have great potential terahertz applications.

2. The absorber design

The unit cell schematics of the proposed absorbers are depicted in Fig. 1, which consist of a patterned metal microstructure, single-layer graphene, a dielectric spacer, and a metallic reflector from the top to the bottom. As a demonstration, we mainly discuss the characteristics of the absorbers with composite graphene and four types of metal microstructure patterns (spiral, ring, disk, and square) in this work. Fig. 1(a) shows the absorber with spiral metal microstructure composed of an Archimedes spiral-shaped strip. Here, we define the origin O (0, 0) as the center point of the inner Archimedes spiral curve, the inner, (x_1, y_1), and outer, (x_2, y_2), curve functions of the Archimedes spirals as follows:

$$\begin{cases} x_1(t) = (-bt)\cos(2\pi t + \pi/2) \\ y_1(t) = (-bt)\sin(2\pi t + \pi/2) \end{cases}, \tag{1}$$

$$\begin{cases} x_2(t) = (-bt + w)\cos(2\pi t + \pi/2) \\ y_2(t) = (-bt + w)\sin(2\pi t + \pi/2) \end{cases}, \tag{2}$$

where b is the turn spacing, and w is the width of the strip, t ranges from 0 to n (the number of turns of the spiral). Fig. 1(b) displays the absorber with a double-ring microstructure, where r_1 and r_2 are the inner and outer radiuses of the small ring, r_3 and r_4 are the inner and outer radiuses of the big ring, respectively. Fig. 1(c) illustrates the absorber with a metal micro-disk with a radius of r_5. Fig. 1(d) depicts the absorber with metal micro-square with a side length s. All of the four types of metal microstructures have the same thickness h_1. The thickness of Topas dielectric spacer and Au reflector are assigned as h_2 and h_3, respectively. The initial values of the geometric parameters are set as $p = 20\,\mu m$, $h_1 = 1\,\mu m$, $h_2 = 60\,\mu m$, $h_3 = 1\,\mu m$, $n = 3$, $w = 0.9\,\mu m$, $b = 2.7\,\mu m$, $r_1 = 3.2\,\mu m$, $r_2 = 5.6\,\mu m$, $r_3 = 6.8\,\mu m$, $r_4 = 7.0\,\mu m$, $r_5 = 1.0\,\mu m$, and $s = 12.0\,\mu m$, as shown in Fig. 1. In the FEM-based simulation, the unit boundary periodic boundary conditions are set in both x and y directions, and the Floquet ports are assigned in z-direction. In the terahertz region, the surface conductivity of graphene is given by Kubo formula as $\sigma_g = \sigma_{intra} + \sigma_{inter}$ (Unit: S) with the intraband and interband contributions [38,39],

$$\sigma_{intra}(\omega, \mu_c, \Gamma, T) = \frac{je^2}{\pi\hbar^2(\omega - j2\Gamma)} \int_0^\infty \left(\frac{\partial f_d(\xi, \mu_c, T)}{\partial \xi} - \frac{\partial f_d(-\xi, \mu_c, T)}{\partial \xi} \right) \xi d\xi, \tag{3}$$

$$\sigma_{inter}(\omega, \mu_c, \Gamma, T) = \frac{je^2(\omega - j2\Gamma)}{\pi\hbar^2} \int_0^\infty \frac{f_d(\xi, \mu_c, T) - f_d(-\xi, \mu_c, T)}{(\omega - j2\Gamma)^2 - 4\xi/\hbar^2} d\xi, \tag{4}$$

where $f_d(\xi, \mu_c, T) = (e^{(\xi - \mu_c)/k_B T} + 1)^{-1}$ is the Fermi-Dirac distribution, ω is the radian frequency, μ_c is the chemical potential or Fermi level, T is the temperature, Γ is the phenomenological scattering rate with $\Gamma = 2\tau^{-1}$, the relaxation time $\tau = \mu_e \mu_c / (e v_F^2)$, μ_e is the electron mobility, v_F is the Femi velocity, e is the charge of an electron, ξ is energy, $\hbar$ is the reduced Plank's constant, and k_B is the Boltzmann's constant. In this study, we assume the temperature $T = 300$ K and the relaxation time of graphene $\tau = 0.05$ ps, which is estimated from the experimentally available graphene carrier mobility [40–42]. All dielectric spacers are assumed to be a lossless polyethylene cyclic olefin copolymer (Topas) with a permittivity of $\varepsilon_d = 2.35$ [43,44] below the graphene sheet and upon the metallic reflector. All metals are modeled as a dispersive gold (Au) using Drude model [45]. The graphene sheet is modeled as an infinite-thin layer with the 2D surface impedance $Z_g = 1/\sigma_g$. The absorbance $A(\omega)$ is calculated from the S-parameters by $A(\omega) = 1 - T(\omega) - R(\omega)$, where the transmission $T(\omega) = |S_{21}|^2$ and reflectance $R(\omega) = |S_{11}|^2$. There is no transmission in these devices because the thickness of gold reflector is much greater than the skin depth of incident wave. Therefore, the absorbance calculation could then be simplified to $A(\omega) = 1 - R(\omega) = 1 - |S_{11}|^2$.

3. Results and discussion

To begin with, we investigate the terahertz absorption performance of the proposed absorber with composite graphene and

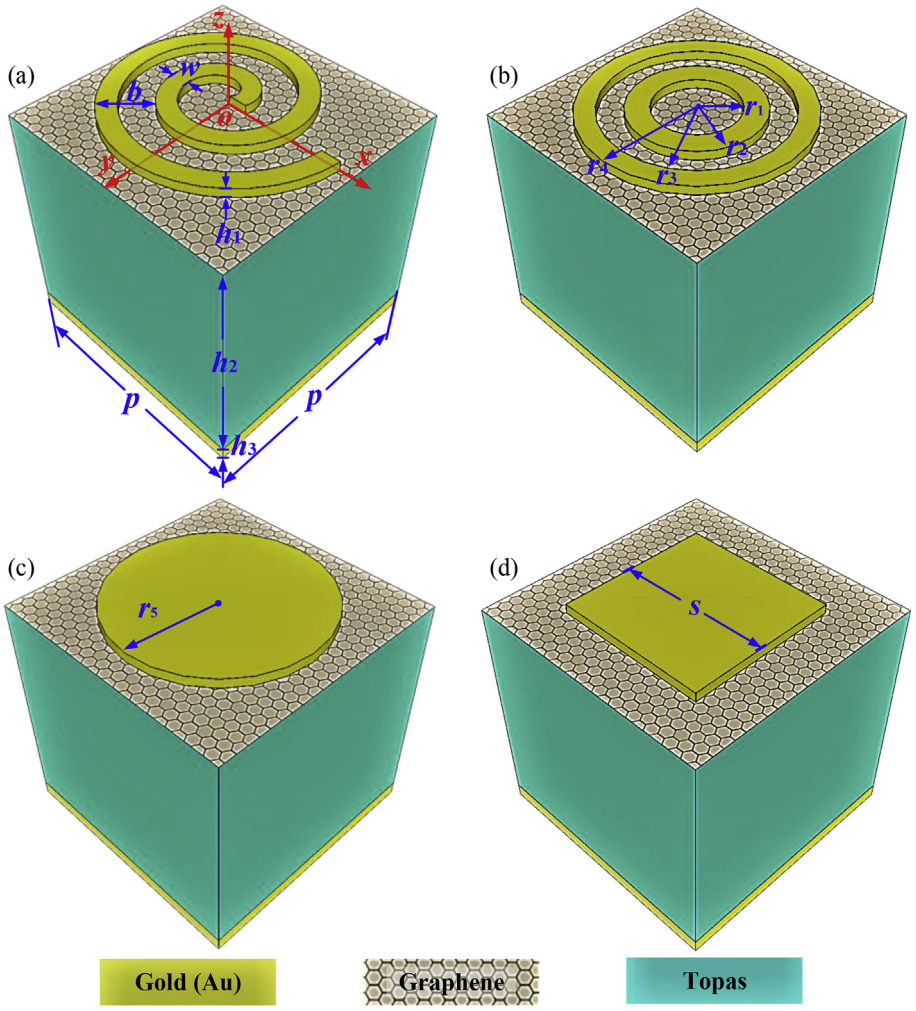

Fig. 1. Schematics of the proposed multiband terahertz absorbers with composite graphene and different metal microstructures. (a) Archimedes spiral microstructure. (b) Double-ring microstructure. (c) Disk microstructure. (d) Square microstructure. The initial dimensions are set as $p = 20\ \mu m$, $h_1 = 1\ \mu m$, $h_2 = 60\ \mu m$, $h_3 = 1\ \mu m$, $n = 3$, $w = 0.9\ \mu m$, $b = 2.7\ \mu m$, $r_1 = 3.2\ \mu m$, $r_2 = 5.6\ \mu m$, $r_3 = 6.8\ \mu m$, $r_4 = 7.0\ \mu m$, $r_5 = 6.0\ \mu m$, and $s = 12.0\ \mu m$. (A colour version of this figure can be viewed online.)

spiral metal microstructure (Fig. 1(a)) under transverse electric (TE) polarization at normal incidence. The chemical potential of graphene is initially assumed to be $\mu_c = 0.5$ eV and the height of Topas spacer (h_2) is set as 60 μm. In this design, a Fabry–Pérot cavity between the continuous graphene and the underneath metal reflector is formed to obtain multiband terahertz absorption, and the periodic gold microstructure array is incorporated to enhance the multiband absorption. As shown in Fig. 2(a), we display the absorption spectra of the proposed absorber (red solid curve) and the modified absorber structures without gold spiral (blue dashed curve) and without graphene sheet (green dot curve) under the same geometric parameters. Clearly, the absorber without the graphene produces almost no absorbance in the whole terahertz frequency range. In the absence of the gold micro-spiral, the absorber demonstrates six absorbance bands between 0 and 10 THz resulted from the graphene and metal reflector Fabry–Pérot resonance. However, the absorbance in each band is not high, and the absorbance peak decreases as the frequency band increases. In contrast, for the proposed absorber with composite graphene and spiral metal microstructure, the six-band absorbance is drastically increased to near unity. The absorbance phenomenon can be understood through the effective medium theory [46]. The real (Re) and imaginary (Im) parts of retrieved normalized effective impedance (Z) of the proposed absorbers without graphene, without spiral metal microstructure, and with composite graphene and spiral metal microstructure are plotted in Fig. 2(b) – (d), respectively. As shown in Fig. 2(b), it is clear that the Z of the proposed absorber without graphene is far from 1, implying no impedance matching between the absorber and the free space. In this case, almost all of the energy of the incident terahertz wave will be reflected back to the free space. The Z of the absorber with graphene changes with the operating frequencies, as shown in Fig. 2(c). It is observed that greater impedance mismatching occurs between the absorber and the free space occurs as the frequency increases to the higher end, which results in the absorbance decreasing at higher absorbance band. While, as shown in Fig. 2(d), it is found that impedance matching between the absorber and the free space is significantly improved by introducing the metal spiral microstructure into the graphene absorber, where the Re (Z) and Im (Z) are approaching 1 and 0 at each absorbance peak frequency, respectively. Therefore, near unity absorbance peaks are achieved because of very small reflectance and no transmission of the absorber at those frequencies.

To study the mechanism of terahertz absorption enhancement, we compare the electric field ($|E|$) distributions of the absorbers with and without spiral gold microstructure under TE polarization,

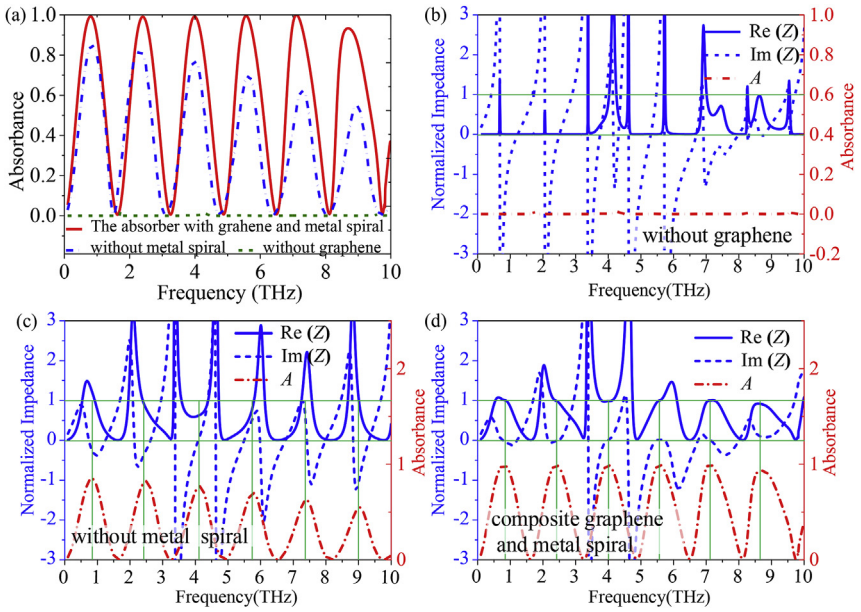

Fig. 2. (a) Comparison of the absorption spectra among the proposed absorbers with composite graphene and spiral metal microstructure, without spiral metal microstructure, and without graphene sheet. (b)–(d) are the retrieved Re (*Z*) and Im (*Z*) of the proposed absorbers without graphene, without spiral metal microstructure, and with composite graphene and spiral metal microstructure, respectively. (A colour version of this figure can be viewed online.)

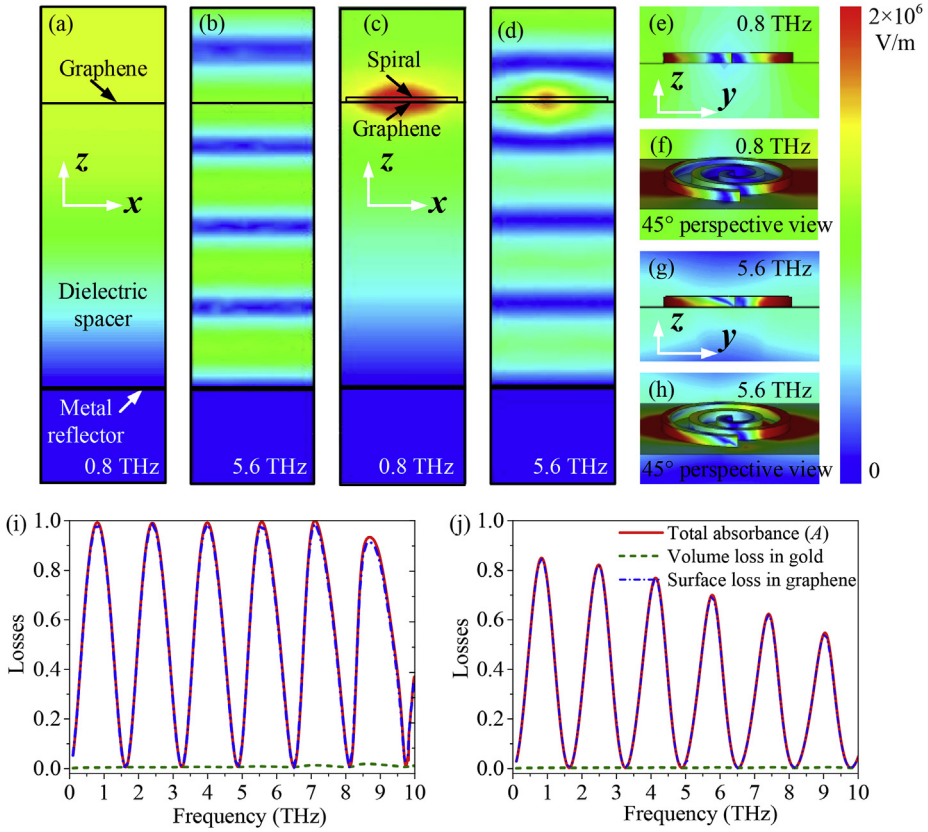

Fig. 3. (a)–(h) are the side-, front-, and 45° perspective-view of the electric field distributions (|*E*|) of graphene absorbers with and without metal spiral microstructure under TE polarization at the first and fourth absorbance peak frequencies of 0.8 and 5.6 THz, respectively. (i) and (j) are the material losses of the proposed graphene absorber with and without metal spiral under TE polarization, respectively. (A colour version of this figure can be viewed online.)

as shown in Fig. 3. Fig. 3(a) and (b) show the side view of $|E|$ distributions on the *xoz* plane of the absorber without gold microstructure at its first and fourth peak resonance frequencies of 0.8 and 5.6 THz, respectively, where the first- and fourth-order Fabry–Pérot resonances are clearly excited between the graphene and metal reflector. The similar first- and fourth-order Fabry–Pérot resonances can also be excited after introducing the metal microstructure, as shown in Fig. 3(c) and (d). The absorber with gold spiral demonstrates obvious $|E|$ enhancement mainly concentrated around gold spiral and graphene sheet. Fig. 3(e) and (f) show the front view and 45° perspective view of the $|E|$ distributions for the absorber with gold spiral, respectively, at the first absorbance peak frequency. Clearly, because of the gold spiral microstructure, much stronger electric fields are concentrated around graphene interface and the terahertz absorption in graphene can be effectively enhanced with respect to the absorber without a gold spiral. A similar phenomenon can be observed at the fourth absorbance peak frequency shown in Fig. 3(g) and (h). Therefore, multiband absorption resulted from the Fabry–Pérot cavity between the continuous graphene and the underneath metal reflector can be effectively enhanced by the plasmon resonance induced by the designed metal microstructures. Fig. 3(i) and (j) show the surface loss of graphene and volume losses of metal of the proposed graphene absorbers with and without gold spiral microstructure. Because we assume Topas is lossless, the absorbance (A) equals to the sum of graphene and gold losses. It is clear that almost whole absorbance in both cases is caused by the graphene loss, while only a negligible part of absorbance is caused by the gold loss due to it acts as a nearly perfect conductor using Drude model in terahertz range. Consequently, by introducing the gold spiral microstructure, the enhanced absorbance of the graphene absorber with gold spiral microstructure results from the increased graphene loss, which can be expected from $|E|$ enhancement around graphene sheet.

The multiband absorption phenomenon of the proposed absorber can be further interpreted by interference theory [47]. In the interference model, the composite graphene and gold spiral array acts as an impedance-tuned air-spacer interface with dramatically modified complex reflection and transmission coefficients shown in Fig. 4(a). Then, the proposed absorber can be decoupled into two tuned interfaces, which are the composite graphene and gold spiral array and the gold reflector located at both sides of the dielectric spacer. As the reflection coefficient of the gold reflector is −1, the total reflection of the absorber is calculated by the superposition the multiple reflections, given by,

$$\tilde{r} = \tilde{r}_{12} - \frac{\tilde{t}_{12}\tilde{r}_{21}e^{i2\tilde{\beta}}}{1+\tilde{r}_{21}e^{i2\tilde{\beta}}} \tag{5}$$

where the reflection coefficients $\tilde{r}_{12} = r_{12}e^{i\phi_{12}}$, $\tilde{r}_{21} = r_{21}e^{i\phi_{21}}$, the transmission coefficients $\tilde{t}_{12} = t_{12}e^{i\theta_{12}}$, $\tilde{t}_{21} = t_{21}e^{i\theta_{21}}$, the transmission phase $\tilde{\beta} = \sqrt{\varepsilon_d}k_0h_2$, and k_0 is the free space wavenumber, respectively. The reflection and transmission coefficients at the spiral-graphene/spacer interface are obtained by simulating the proposed absorber unit cell with a dielectric spacer but without gold reflector plate, as shown in Fig. 4(b) and (c). Then, the absorbance spectra can be calculated by $A(w) = 1 - |\tilde{r}(w)|^2$. As shown in Fig. 4(d), the absorbance spectrum of the proposed absorber with 60 μm thick spacer obtained from the interference theory is consistent well with numerical simulations.

To better understand the physical origin of the absorber, we further study the general effect of the Topas spacer on the multiband terahertz absorption characteristics. As we know, the spacer thickness h_2 plays a major role in determining the wavelength of the graphene-metal reflector Fabry–Pérot resonances. Here, we present and compare the absorption spectra of the absorber as a function of the thickness h_2 using interference theory and numerical simulation, as shown in Fig. 5(a). It is clear that the spacer thickness (h_2) directly affects the number of absorbance peaks. As

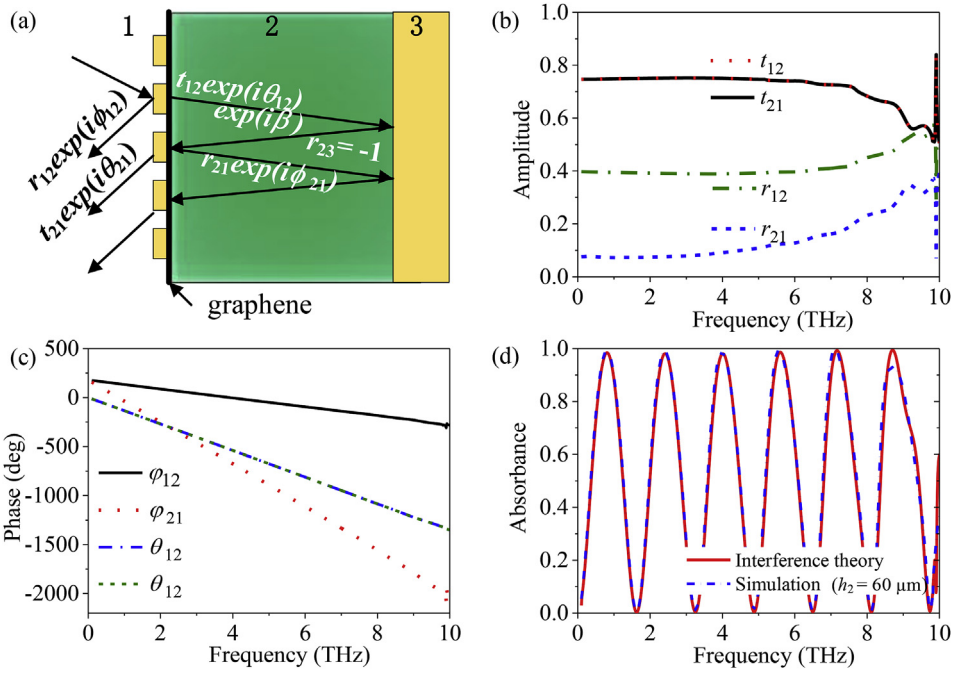

Fig. 4. (a) Multiple reflections interference model of the proposed absorber. (b) Amplitude and (c) Phase of the reflection and transmission coefficients obtained from proposed absorber unit cell with a dielectric spacer but without gold reflector plate under $h_2 = 60$ μm, respectively. (e) Comparison of the interference theory (Theo.) and simulation (Sim.) absorption spectra of the proposed absorber with the dielectric spacer thickness of $h_2 = 60$ μm. (A colour version of this figure can be viewed online.)

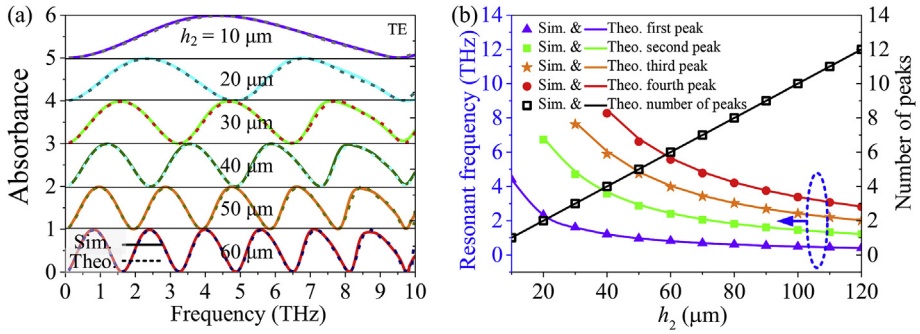

Fig. 5. (a) The interference theory (Theo.) and simulation (Sim.) absorption spectra of the proposed absorber with different thickness of Topas spacer ranging from 10 to 60 μm. (b) Dependence of the absorbance peak frequency and the number of peaks on the thickness h_2 ranging from 10 to 120 μm. (A colour version of this figure can be viewed online.)

h_1 increases from 10 to 60 μm, the number of absorbance peaks increases from 1 to 6, correspondingly. The multiple reflections in the absorber, the maximum absorbance (constructive interference) and minimum absorbance (destructive interference) occur at phase condition of $\Delta\phi = 2\tilde{\beta} + \phi_{21} + \phi_{23} = 2m\pi$ and $\Delta\phi = (2m\text{-}1)\ \pi$, respectively, where ϕ_{21} represents the reflection phase shift on the graphene-Topas interface shown in Fig. 4(c), and ϕ_{23} is the reflection phase shift on Topas-metal reflector interface ($\phi_{23} = \pi$), m is a positive integer. The dependence of the theoretical and simulated the lowest four absorbance peak frequencies and the total number of peaks between 0 and 10 THz on the thickness h_2 ranging from 10 to 120 μm are shown in Fig. 5(b). It is clear that the interference theory not only can predict the absorbance peaks but also can obtain the exact shapes of absorbance spectra, which is in

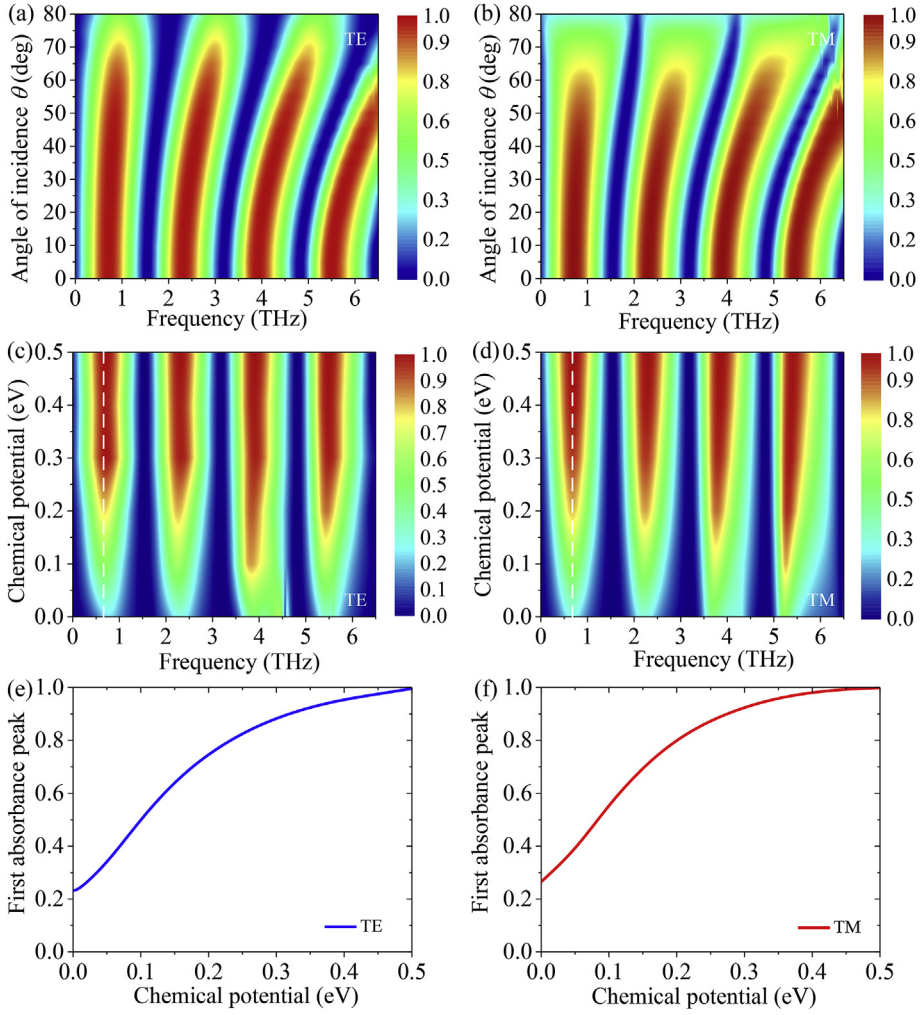

Fig. 6. Dependence of absorption spectra of the proposed absorber on the terahertz incidence angle (θ) ranging from 0° to 80° and graphene chemical potential (μ_c) ranging from 0 to 0.5 eV. (a) Absorption spectra as a function of θ under TE polarization. (b) Absorption spectra as a function of θ under TM polarization. (c) Absorption spectra as a function of μ_c under TE polarization. (d) Absorption spectra as a function of μ_c under TM polarization. (e) First absorbance peak (see the white dashed line in (c)) as a function of μ_c under TE polarization. (f) First absorbance peak (see the white dashed line in (d)) as a function of μ_c under TM polarization. (A colour version of this figure can be viewed online.)

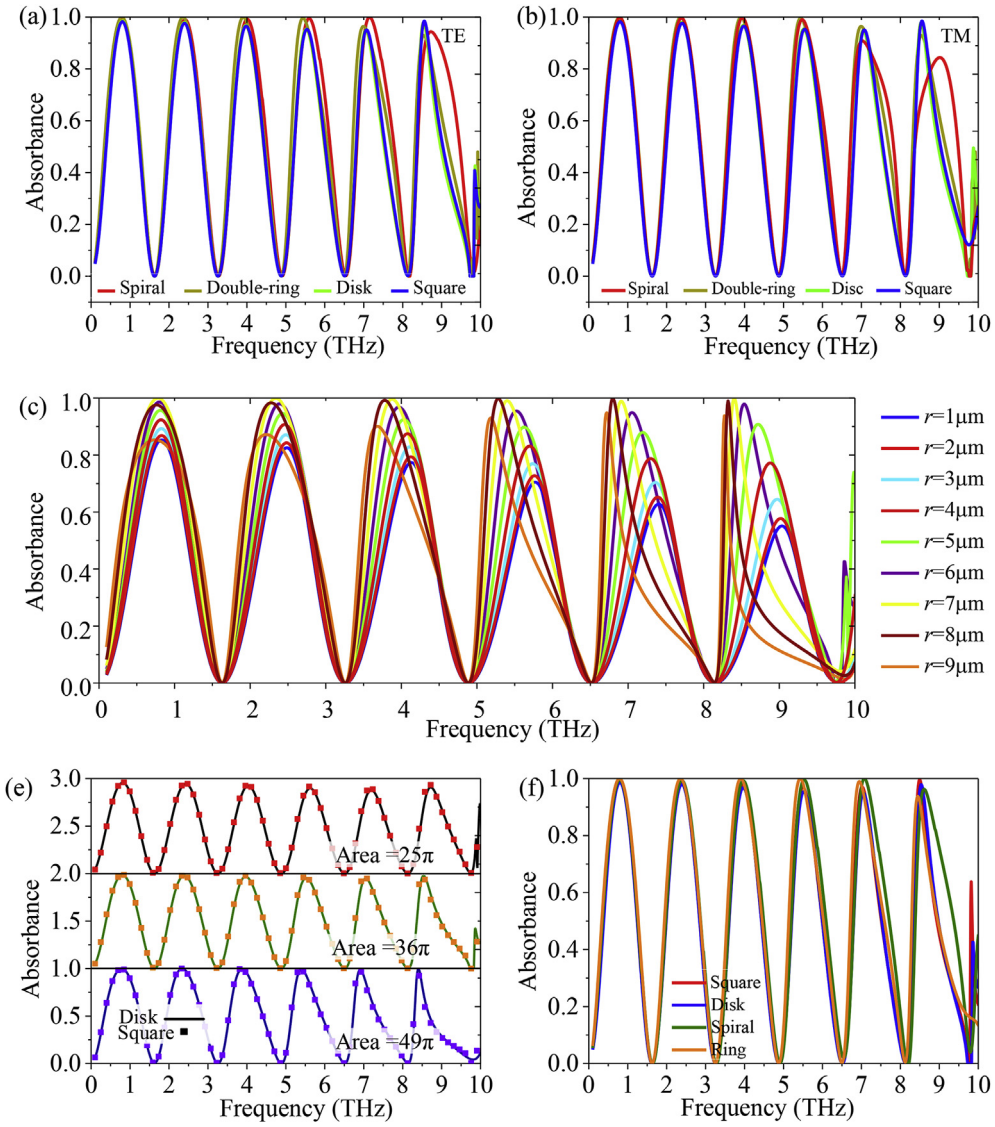

Fig. 7. The absorption spectra of the proposed absorbers with different microstructures of the Archimedes spiral, double-ring, disk, and square under TE polarization (a) and TM polarization (b). (c) Dependence of absorbance spectra of the graphene absorbers with metal disk microstructure on the radius. (d) Absorbance spectra of graphene absorbers with disk and square microstructure at the same area of 25π, 36π, and 49π μm^2. (e) Absorbance spectra of graphene absorbers with four microstructures at the same area of 36π μm^2. (A colour version of this figure can be viewed online.)

excellent agreement with simulations. As h_2 increases, the number of peaks increases linearly and the frequency of each order resonance decreases correspondingly, where the redshift of the lower absorbance peak is slower and the redshift of the higher absorbance peaks is faster in 0–10 THz. Therefore, by reasonably setting the height of the dielectric spacer, the proposed absorber can achieve an arbitrary number of absorption bands in the entire terahertz range.

Then, we investigate the dependence of the absorption characteristics of the proposed absorber with composite graphene and gold spiral microstructure on the incidence angle and the chemical potential of graphene. To simplify the analysis, we set Topas thickness (h_3) of 60 μm and keep other parameters fixed as the initial values. The absorption spectra as a function of frequency and incidence angle under TE and transverse magnetic (TM) polarizations are illustrated in Fig. 6(a) and (b), respectively. It is found that the first absorption band shows a good angular stability under both polarizations, while the rest of absorption bands show a certain degree of blue shift as the angle increases, and more obvious blue shift when the incidence angle is larger than 10°. Especially, the first absorption band exhibits excellent angular stability, and the absorbance peak remains over 90% even at a large incidence angle of 60°. Furthermore, the effects of graphene chemical potential (μ_c) on the absorption characteristics under TE and TM polarizations are shown in Fig. 6(c) and (d). Clearly, graphene chemical potential has a significant impact on the absorption of the absorber. For example, by adjusting μ_c from 0 to 0.5 eV, the absorbance peak of the first absorption band increases from 23.18 (26.50) to 99.59 (99.88) % for TE (TM) polarization, as shown in Fig. 6e, f. Therefore, if we set μ_c as 0 and 0.5 eV as the "OFF" and "ON" states, respectively, the absorber can be applied as a photoelectric switch with over 73% absorption switching property for both polarizations.

Finally, to study the influence of the gold microstructure shapes on the plasmonic response of the graphene, we simulate and compare the absorption of proposed absorbers with four different type microstructures of the spiral, ring, disk, and square under the

same initial geometric parameters (see Fig. 1), whose areas are 19.8π, 35.6π, 36π, and 144 (or 45.9π) μm^2, respectively. Interestingly, similar absorption spectra are obtained regardless of the microstructure shapes of the absorbers under TE and TM polarizations, as depicted in Fig. 7(a) and (b). All of the four different metal microstructures can efficiently enhance absorption, achieve near unity absorption characteristics at the same frequency, and possess polarization independent under normal incidence. In other words, multi-resonance absorption in graphene caused by Fabry–Pérot cavity can be greatly enhanced to near-unity using the graphene-based absorbers with various different metal microstructures. To better understand the insensitivity of absorbance of the proposed absorbers, we further study the effects of geometric parameters of the microstructure on the absorbance spectra. Fig. 7(c) shows the absorbance spectra for TE polarization of the graphene absorber with metal disk under different radius. It is found that the absorbance spectra change a lot as the radius greatly varies from 1 to 9 μm. However, by selecting the moderate $r = 5, 6, 7$ and 8 μm, corresponding area occupation ratio ranging from 20% ($r = 5$, $p = 20$, ratio of 25π/400) to 50% ($r = 8$, $p = 20$, ratio of 64π/400), the six absorption peaks can be simultaneously enhanced to near unity while neglecting the bandwidth changing at higher resonance frequencies. It is worth noting that the area occupation ratio of the 2D arranged metal microstructures plays an important role in determining the absorbance enhancement and influencing the shape of the spectra. By setting the same area of 25π, 36π, and 49π μm^2 for both metal square and disk microstructures, as shown in Fig. 7(d), completely coincide absorbance spectra for these two kinds of graphene absorbers are obtained, showing excellent shape insensitivity. Based on this point, the absorbance enhancement in the absorbers is less sensitive to the shapes but more sensitive dimensions. Furthermore, by setting the same area of 36π for all four kinds of microstructures, similar absorbance spectra are achieved, as shown in Fig. 7(e), where the absorbance spectra of the proposed absorbers with identical areas show better consistency than that with different microstructure areas shown in Fig. 7(a). Considering the robust absorbance insensitivity to the geometric parameters, small manufacturing errors of the device will only cause a negligible influence on its multiband absorption, which may alleviate fabrication difficulty in device realization.

4. Conclusion

In this work, an effective method to enhance multi-band absorption and a variety of tunable polarization-insensitive multiband terahertz multiband absorbers based on composite graphene and metal microstructures have been numerically demonstrated. In these devices, multiband absorption resulted from the Fabry–Pérot cavity between the continuous graphene and the underneath metal reflector can be effectively enhanced by the plasmon resonance induced by the designed metal microstructures. The number of absorption bands can be adjusted at will by tuning the height of the dielectric spacer. As a demonstration, we performed numerical simulations on four multi-band absorbers based on composite graphene and four types of metal microstructure patterns (spiral, ring, disk, and square). Interestingly, all absorbers exhibit the same absorption properties with six near-unity absorbance bands over the entire terahertz region regardless of the shapes of microstructures. These absorbers also show clear independence of polarization under normal incidence, and their absorbance peaks can be flexibly controlled by changing the graphene chemical potential. The proposed method is of great significance and provides a guide to enhance the graphene absorption, the presented absorbers also possess great potential applications in terahertz photoelectric detectors, sensors, modulators, and switches.

Acknowledgments

This work was supported by National Natural Science Foundation of China (61601393) and Shenzhen Science and Technology Project (JCYJ20180306172733197).

References

[1] H.J. Song, T. Nagatsuma, Present and future of terahertz communications, IEEE Tran. Terahertz Sci. and Technol. 1 (1) (2011) 256–263.
[2] M. Tonouchi, Cutting-edge terahertz technology, Nat. Photon. 1 (2007) 97–105.
[3] H. Shigekawa, S. Yoshida, O. Takeuchi, Spectroscopy: nanoscale terahertz spectroscopy, Nat. Photon. 8 (2014) 815–817.
[4] N.I. Landy, S. Sajuyigbe, J.J. Mock, D.R. Smith, W.J. Padilla, A perfect metamaterial absorber, Phys. Rev. Lett. 100 (20) (2008), 207402.
[5] S. Thongrattanasiri, F.H. Koppens, F.J. García de Abajo, Complete optical absorption in periodically patterned graphene, Phys. Rev. Lett. 108 (4) (2012), 047401.
[6] L. Ye, Y. Chen, G.Y. Cai, N. Liu, J. Zhu, Z. Song, et al., Broadband absorber with periodically sinusoidally-patterned graphene layer in terahertz range, Optic Express 25 (10) (2017) 11223–11232.
[7] S. Ogawa, M. Kimata, Metal-insulator-metal-based plasmonic metamaterial absorbers at visible and infrared wavelengths: a review, Materials 11 (3) (2018) 458.
[8] B.T. Kearney, F. Alves, D. Grbovic, G. Karunasiri, Al/SiOx/Al single and multiband metamaterial absorbers for terahertz sensor applications, Opt. Eng. 52 (1) (2013), 013801.
[9] B. Appasani, P. Prince, R.K. Ranjan, N. Gupta, V.K. Verma, A simple multi-band metamaterial absorber with combined polarization sensitive and polarization insensitive characteristics for terahertz applications, Plasmonics 1–6 (2018).
[10] B.X. Wang, G.Z. Wang, Quad-Band terahertz absorber based on a simple design of metamaterial resonator, IEEE Photon. J. 8 (6) (2016) 1–8.
[11] B.X. Wang, G.Z. Wang, T. Sang, L.L. Wang, Six-band terahertz metamaterial absorber based on the combination of multiple-order responses of metallic patches in a dual-layer stacked resonance structure, Sci. Rep. 7 (2017) 41373.
[12] K.S. Novoselov, V.I. Fal'ko, L. Colombo, P.R. Gellert, M.G. Schwab, et al., A roadmap for graphene, Nature 490 (7419) (2012) 192–200.
[13] T. Low, P. Avouris, Graphene plasmonics for terahertz to mid-infrared applications, ACS Nano 8 (2) (2014) 1086–1101.
[14] A.N. Grigorenko, M. Polini, K.S. Novoselov, Graphene plasmonics, Nat. Photon. 6 (11) (2012) 749–758.
[15] F.H. Koppens, D.E. Chang, F.J. García de Abajo, Graphene plasmonics: a platform for strong light-matter interactions, Nano Lett. 11 (8) (2011) 3370–3377.
[16] Thomas Mueller, Fengnian Xia, Phaedon Avouris, Graphene photodetectors for high-speed optical communications, Nat. Photon. 4 (5) (2010) 297–301.
[17] F. Xia, M. Thomas, Y. Lin, A. Valdes-Garcia, P. Avouris, Ultrafast graphene photodetector, Nat. Nanotechnol. 4 (12) (2009) 839–843.
[18] X. Wang, Z. Cheng, K. Xu, H. Tsang, J. Xu, High-responsivity graphene/silicon-heterostructure waveguide photodetectors, Nat. Photon. 7 (11) (2013) 888–891.
[19] A. Yu Nikitin, F. Guinea, F.J. García-Vidal, L. Martín-Moreno, Edge and waveguide THz surface plasmon modes in graphene micro-ribbons, Phys. Rev. B 84 (16) (2011) 1401–1408.
[20] M. Liu, X. Yin, E. Ulin-Avila, A graphene-based broadband optical modulator, Nature 474 (7349) (2011) 64–67.
[21] L. Ye, K. Sui, Y. Liu, M. Zhang, Q.H. Liu, Graphene-based hybrid plasmonic waveguide for highly efficient broadband mid-infrared propagation and modulation, Optic Express 26 (12) (2018), 15935-15847.
[22] L. Ye, K. Sui, Y. Zhang, Q.H. Liu, Broadband optical waveguide modulators based on strongly coupled hybrid graphene and metal nanoribbons for near-infrared applications, Nanoscale 11 (2019) 3229–3239.
[23] L. Luo, K. Wang, C. Ge, K. Guo, F. Shen, Z. Yin, Z. Guo, Actively controllable terahertz switches with graphene-based nongroove gratings, Photon. Res. 5 (2017) 604–611.
[24] Z. Yin, Q. Zheng, K. Wang, K. Guo, F. Shen, H. Zhou, Y. Sun, Q. Zhou, J. Gao, L. Luo, Z. Guo, Tunable dual-band terahertz metalens based on stacked graphene metasurfaces, Optic Commun. 429 (2018) 41–45.
[25] Z. Guo, X. Nie, F. Shen, H. Zhou, Q. Zhou, J. Gao, K. Guo, Actively tunable terahertz switches based on subwavelength graphene waveguide, Nanomaterials 8 (9) (2018) 665.
[26] L. Luo, K. Wang, K. Guo, F. Shen, X. Zhang, Z. Yin, Z. Guo, Tunable manipulation of terahertz wavefront based on graphene metasurfaces, J. Opt. 19 (11) (2017), 115104.
[27] P. Chen, A. Alu, Terahertz metamaterial devices based on graphene nanostructures, IEEE Trans. Terahertz Sci. Tech. 3 (6) (2013) 748–756.
[28] L. Ye, F. Zeng, Y. Zhang, X. Xu, X. Yang, Q.H. Liu, Frequency-reconfigurable wide-angle terahertz absorbers using single- and double-layer decussate graphene ribbon arrays, Nanomaterials 8 (10) (2018) 834.
[29] L. Ye, X. Chen, J. Zhuo, F. Han, Q.H. Liu, Actively tunable broadband terahertz absorption using periodically square-patterned graphene, APEX 11 (10) (2018), 102201.

[30] L. Ye, X. Chen, G.Y. Cai, J. Zhu, N. Liu, Q.H. Liu, Electrically tunable broadband terahertz absorption with hybrid-patterned graphene metasurfaces, Nanomaterials 8 (8) (2018) 562.
[31] M. Amin, M. Farhat, H. Bağcı, An ultra-broadband multilayered graphene absorber, Optic Express 21 (24) (2013) 29938–29948.
[32] A.Y. Zhu, F. Yi, J.C. Reed, Cavity-enhanced mid-infrared absorption in perforated graphene, J. Nanophotonics 8 (1) (2014), 083888.
[33] J. Zhang, J. Tian, L. Li, A dual-band tunable metamaterial near-unity absorber composed of periodic cross and disk graphene arrays, IEEE Photon. J. 10 (2) (2018), 1943-0655.
[34] G. Yao, F. Ling, Y. Gang, Dual-band tunable perfect metamaterial absorber in the THz range, Optic Express 24 (2) (2016) 1518–1527.
[35] Q. Zhou, P. Liu, L. Bian, X. Cai, H. Liu, Multi-band terahertz absorber exploiting graphene metamaterial, Opt. Mater. Express 8 (2018) 2928–2940.
[36] R. Gao, Z. Xu, C. Ding, J. Yao, Intensity-modulating graphene metamaterial for multiband terahertz absorption, Appl. Opt. (2016) 551929–551933.
[37] Z. Wang, Y. Hou, Ultra-multiband absorption enhancement of graphene in a metal-dielectric-graphene sandwich structure covering terahertz to mid-infrared regime, Optic Express 25 (16) (2017) 19185–19194.
[38] G.W. Hanson, Dyadic Green's functions and guided surface waves for a surface conductivity model of graphene, J. Appl. Phys. 103 (6) (2008), 064302.
[39] G.W. Hanson, Dyadic Green's functions for an anisotropic, non-local model of biased graphene, IEEE Trans. Antennas Propag. 56 (3) (2008) 747–757.
[40] K. Bolotin, K. Sikes, Z. Jiang, M. Klima, G. Fudenberg, J. Hone, P. Kima, H. Stormer, Ultrahigh electron mobility in suspended graphene, Solid State Commun. 146 (2008) 351–355.
[41] W.L. Gao, J. Shu, C.Y. Qiu, Q.F. Xu, Excitation of plasmonic waves in graphene by guided-mode resonances, ACS Nano 6 (9) (2012) 7806–7813.
[42] C.R. Dean, A.F. Young, I. Meric, C. Lee, L. Wang, S. Sorgenfrei, K. Watanabe, T. Taniguchi, P. Kim, K.L. Shepard, J. Hone, Boron nitride substrates for high-quality graphene electronics, Nat. Nanotechnol. 5 (2010) 722–726.
[43] Faraji Mahboobeh, M.K. Moravvej-Farshi, L. Yousefi, Tunable THz perfect absorber using graphene-based metamaterials, Optic Commun. 355 (2015) 352–355.
[44] J.S. Gómez-Díaz, M. Esquius-Morote, J. Perruisseau-Carrier, "Plane wave excitation-detection of nonresonant plasmons along finite-width graphene strips, Optic Express 21 (21) (2013) 24856–24872.
[45] M.A. Ordal, L.L. Long, R.J. Bell, S.E. Bell, R.R. Bell, R.W. Alexander, et al., Optical properties of the metals Al, Co, Cu, Au, Fe, Pb, Ni, Pd, Pt, Ag, Ti, and W in the infrared and far infrared, Appl. Opt. 2 (7) (1983) 1099–1119.
[46] D.R. Smith, D.C. Vier, T. Koschny, C.M. Soukoulis, Electromagnetic parameter retrieval from inhomogeneous metamaterials, Phys. Rev. E 71 (2005), 036617.
[47] H.T. Chen, Interference theory of metamaterial perfect absorbers, Optic Express 20 (7) (2012) 7165–7172.